High-Density and High-Coverage Composite Atrial Activation Maps: An In-Silico Validation Study

Ozan Özgül, Victor G. Marques, Ben JM Hermans, Arne van Hunnik, Sander Verheule, Ali Gharaviri, Simone Pezzuto, Angelo Auricchio, Ulrich Schotten, Pietro Bonizzi, and Stef Zeemering

***Abstract*—Objective: Repetitive atrial activation patterns (RAAPs) during complex atrial tachycardia could be associated with localized mechanisms that can be targeted. Clinically available electroanatomical mapping systems are limited by either the spatial coverage or electrode density of the mapping catheters, preventing the adequate visualization of transiently occurring RAAPs. This work proposes a technique to overcome this shortcoming by stitching spatially overlapping conduction patterns together to a larger image- called a composite map. Methods: Simulated stable mechanisms and meandering reentries are sequentially mapped (4 × 4 grid, 3 mm spacing) and then reconstructed back to the original sizes with the proposed recurrence plot-based algorithm. Results: The reconstruction of single linear waves presents minimal errors (local activation time (LAT) difference: 3.2 [1.6–4.9] ms, conduction direction difference: 5.2 [2.3–8.0] degrees). Errors significantly increase ($p<0.05$) for more complex patterns, being the highest with unstable reentries (LAT difference: 10.3 [3.5–16.2] ms, conduction direction difference: 18.2 [6.7–29.7] deg). In a second part of the analysis, 111 meandering reentries are reconstructed. Mapping 30 locations overlappingly around each reentry core was found to be the optimal mapping strategy. For this optimal setting, LAT, conduction direction, and core localization errors are low (6.1 [4.2–8.6] ms, 11.2 [8.6–15.5] deg and 4.1 [2.9–4.9] mm, respectively) and are weakly correlated with the degree of the meander ($\rho = 0.41$, $\rho = 0.40$ and $\rho = 0.20$, respectively). Conclusion: Our findings underline the feasibility of generating composite maps by stitching spatially overlapping recordings. Significance: Composite maps can be instrumental in personalized ablation strategies.**

***Index Terms*—Atrial arrhythmias, catheter ablation, conduction patterns, high-density atrial mapping, recurrence plots, repetitive activation patterns, sequential mapping.**

I. Introduction

CATHETER ablation of the pulmonary veins has become a first-line therapeutic approach for patients with atrial fibrillation (AF) [1], with an increasing number of procedures being conducted each year [2]. However, many patients may still experience recurrences of atrial tachycardias after pulmonary vein isolation (PVI), including episodes of AF and both typical and atypical atrial flutters (AFL) [3]. These new-onset arrhythmias may be either byproducts of the ablative lesions or a priori drivers that remained masked until other sources were eliminated [4]. Regardless of the underlying pathophysiology, these arrhythmias require additional mapping and ablation procedures for an increasing number of patients, highlighting the need for more efficient mapping approaches [5].

Clinical mapping catheters with high electrode density lack extensive spatial coverage, making it infeasible to simultaneously map the entire atrium, which is essential for a thorough electrophysiological assessment [6]. For highly stable arrhythmias, this problem is overcome by combining information from multiple cycles using a reference catheter, typically in the coronary sinus (CS). However, post-ablation ATs may be maintained by a complex combination of ectopic foci, and functional and anatomical reentries, which may not be well reflected by the reference catheter due to beat-to-beat variability and competing mechanisms [7]. Atrium-wide mapping technologies have been developed to address the poor spatial coverage problem, such as panoramic mapping with basket catheters [8], non-contact charge density mapping [9], and electrocardiographic imaging

Manuscript received 14 December 2023; revised 13 April 2024 and 20 July 2024; accepted 27 July 2024. Date of publication 6 August 2024; date of current version 16 January 2025. This work was supported in part by the European Union under (PersonalizeAF) Grant 860974 and (MAESTRIA) Grant 965286, in part by the Swiss National Supercomputing Centre under Project s1074, and in part by the Dutch Heart Foundation under (EmbRACE) Grant 01-002-2022-0118. *(Ozan Özgül and Victor G. Marques contributed equally to this work.) (Corresponding author: Stef Zeemering.)*

Ozan Özgül, Victor G. Marques, Ben JM Hermans, Arne van Hunnik, Sander Verheule, and Ulrich Schotten are with the Department of Physiology, Maastricht University, The Netherlands.

Ali Gharaviri is with the Centre for Cardiovascular Science, University of Edinburgh, U.K.

Simone Pezzuto is with the Department of Mathematics, University of Trento, Italy.

Angelo Auricchio is with the Center for Computational Medicine in Cardiology, Università della Svizzera italiana, Switzerland.

Pietro Bonizzi is with the Department of Advanced Computing Sciences, Maastricht University, The Netherlands.

Stef Zeemering is with the Department of Physiology, Cardiovascular Research Institute Maastricht, Maastricht University, 6200 MD Maastricht, The Netherlands (e-mail: s.zeemering@maastrichtuniversity.nl).

This article has supplementary downloadable material available at https://doi.org/10.1109/TBME.2024.3439502, provided by the authors.

Digital Object Identifier 10.1109/TBME.2024.3439502

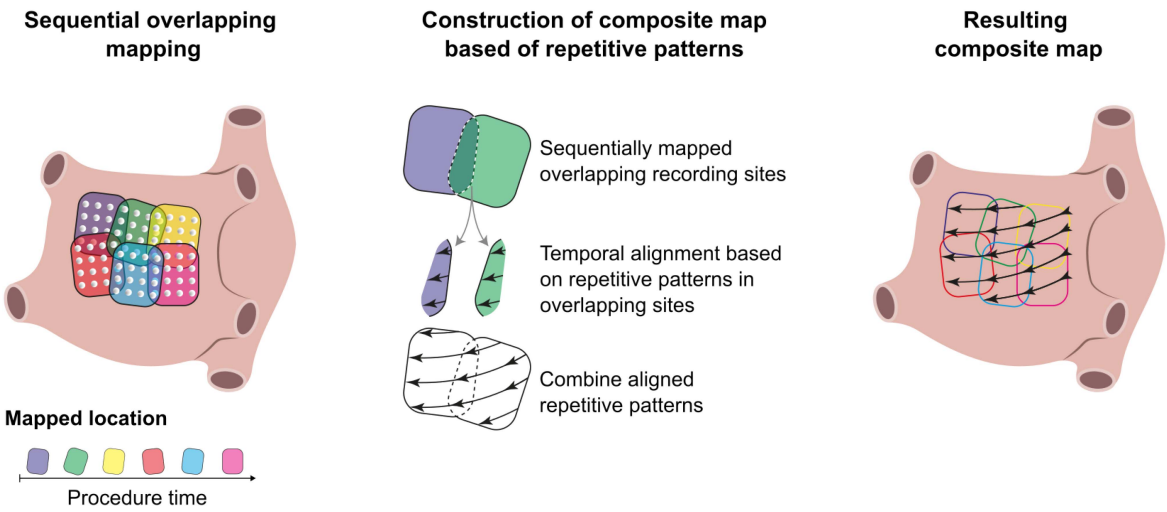

Fig. 1. Schematic description of the composite mapping approach for high-density and high-coverage activation maps (posterior view of atria).

(ECGi) [10] as well as computational mapping strategies [11], [12]. However, these techniques either suffer from reduced electrode density [8] or inaccuracies due to challenges in solving inverse problems [13].

As a potential solution, we have proposed composite mapping computational tool for generating high-coverage and high-density atrial activation maps for repetitive patterns [14]. Arrhythmogenic drivers such as focal and rotational activities are often repetitive and are also expected to entrain their close vicinity and lead to repetitive atrial activation patterns (RAAPs) [15], [16], [17]. Such repetitive patterns can be detected at multiple sites and utilized to align and combine patterns for a larger view. Composite maps are generated by merging ('stitching together') activation maps of prevailing conduction obtained in spatially overlapping catheter positions without relying on a CS reference catheter. In the presence of a repetitive arrhythmogenic driver, this prevailing activation pattern is expected to capture the driver-related activation activity in a larger area. We have previously explored the feasibility of this method in a goat model of AF, where we mimicked sequential, overlapping recordings by segmenting a large epicardial grid into spatially overlapping smaller regions [14]. However, the application of the algorithm in a realistic mapping setting by mapping actual repetitive mechanisms has not yet been investigated.

In this work, we reproduced realistic scenarios through an in-silico experimental setting, where stable and unstable mechanisms were simulated, sequentially mapped in an overlapping manner with an in-silico version of a clinically available catheter, and reconstructed using the composite mapping algorithm. We calculated reconstruction errors in terms of local activation times (LATs), electrode-specific conduction directions, and the detected mechanism locations. Moreover, we assessed the performance of the algorithm in scenarios with increased spatiotemporal instability due to the meandering behavior of repetitive drivers, which is frequently observed during atrial arrhythmia [18]. Finally, we investigated the degree of overlap between sequential recordings required to generate accurate composite maps.

II. Methods

A. Composite Mapping Algorithm

When mapping the atria sequentially, there will be spatial overlaps between catheter positions (different colors in Fig. 1, left). Such overlaps present an opportunity to connect activation patterns over multiple catheter positions, analogous to the stitching of spatially overlapping photographs to obtain a panoramic photo. The spatiotemporal similarity of the RAAPs detected in the overlapping area between two catheter positions (e.g., purple and green areas in Fig. 1) can be utilized to determine if the same RAAPs were observed in two different positions and, if so, temporally align them (Fig. 1, middle). Repeating this for more than two catheter positions allows a network of connected RAAPs over different locations to be stitched together. The resultant map is coined as a composite map (Fig. 1, right).

Three steps are necessary to create a composite map: (i) detection of RAAPs in each catheter position, (ii) comparing detected RAAPs in overlapping pairs based on the conduction patterns in the overlapping area, and (iii) identifying the network of connected RAAPs (RAAP connectivity graph) over multiple catheter positions. These steps are introduced in the next section.

1) RAAP Detection With Recurrence Plots: A recurrence plot is a square symmetric matrix that visualizes recurrences (similar values) between all time point pairs, (i, j) [19]. In a recurrence plot, recurrence $R_{i,j} \in \{0, 1\}$ between two time points of a time series, $\vec{x}(i)$ and $\vec{x}(j)$, occurs when the distance between these points is smaller than a threshold ϵ:

$$R_{i,j} = \mathcal{H}(\varepsilon - D(\vec{x}(i), \vec{x}(j))), \tag{1}$$

with $\mathcal{H}$ the Heaviside step function, ϵ the threshold and D the distance function.

We previously demonstrated that recurrence plots can be used to detect RAAPs during complex atrial arrythmias [15], [16], [20]. For this, first, LATs in the unipolar electrograms were detected using template matching and a probabilistic assignment algorithm based on the estimated activation cycle length distribution [21]. To mitigate false LATs detections caused by the far-field effects on unipolar electrograms, we

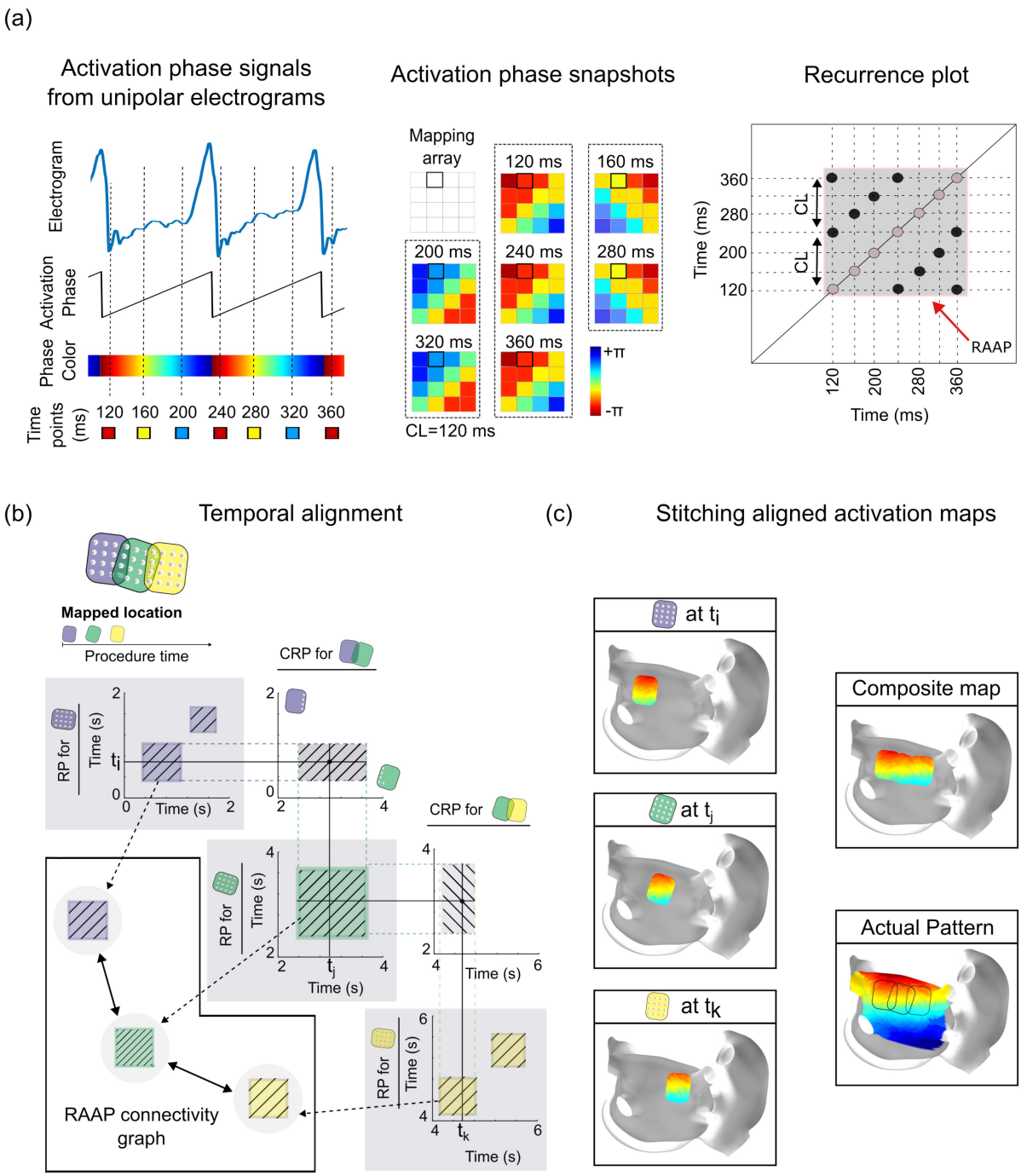

Fig. 2. Methods: (a) Unipolar electrograms were annotated, transformed to activation-phase signals, and used to generate activation-phase snapshots. Time points with similar activation phase snapshots were marked in a recurrence plot (RP). A repetitive atrial activation pattern (RAAP) is represented in the RP by a square block of diagonal entries, each separated by one cycle length. (b) RAAPs detected on individual overlapping catheter locations (purple, green and yellow) show high recurrence in cross-recurrence plots obtained by the electrodes within the overlapped area. A RAAP connectivity graph depicts the connected RAAPs among different catheter positions. A time point in any catheter position can be traced over different positions using the recurrence points in recurrence/cross recurrences (c) Associated activation phase snapshots are connected over multiple catheter locations to form a composite map.

selected LATs that were also present in bipolar electrogram. Next, intervals between consecutive LATs on each electrode were linearly interpolated with phase values between [-π, π) (Fig. 2(a), left). ψ_t^k, the output of the phase interpolation process, represents the activation-phase value of the electrode k at the time t. Repeating this for all electrodes, we created an activation phase snapshot: an image representing activation phase values at a single time point over all electrodes on the catheter (Fig. 2(a), middle).

The distance $\delta_{i,j}$ between two activation-phase snapshots at time points i and j was quantified by averaging the differences in the cosine of the phase angles across all N electrodes. This

average was then expressed as a fraction of the activation-phase duration of a single activation cycle (2π):

$$\delta_{i,j} = \frac{1}{2\pi} cos^{-1}\left(\frac{1}{N}\sum_{k=1}^{N}\cos\left(\psi_i^k - \psi_j^k\right)\right) \quad (2)$$

where ψ_i^k stands for the activation-phase value of the electrode k at the time i. Two snapshots perfectly in phase or in oppositional phase (out of the phase of a full activation cycle length) yield $\delta_{i,j} = 0$, and if they are out of phase by half the length of an activation cycle, $\delta_{i,j} = 0.5$. Based on this distance metric, (1) can be rewritten:

$$R_{i,j} = \begin{cases} 0, & \delta_{i,j} > \delta_{thr} \\ 1, & \delta_{i,j} \leq \delta_{thr} \end{cases} \quad (3)$$

with δ_{thr} the recurrence threshold chosen in accordance with [16]. Fig. 2(a) depicts an exemplary case. The snapshots at 180 and 300 ms showed high similarity (Fig. 2(a), middle). As a result, positions (180, 300) and (300, 180) were marked as a recurrence in the recurrence plot (Fig. 2(a), right).

RAAPs were characterized by square block structures around the main diagonal of a recurrence plot (Fig. 2(a), right) as a consequence of the reappearance of the same activation phase snapshot over consecutive cycles. To determine the presence of a RAAP, we computed the recurrence rate (RR) or the density of the recurrence points in the recurrence plot during the time course of the RAAP. RR for two time intervals, S and T, was defined as:

$$\begin{aligned} \mathrm{RR}(S,T) &= CL \times \frac{\sum_{i\in S}\sum_{j\in T} R_{i,j}}{|S|\,|T|}, \\ \text{s.t.} \quad S &= [s_{\text{start}}, s_{\text{end}}], \\ T &= [t_{\text{start}}, t_{\text{end}}] \end{aligned} \quad (4)$$

with CL being the cycle length in samples and $s_{start}, t_{start}, s_{end}, t_{end}$ being the start and the end time sample indices for both time intervals, respectively. A pattern, spanning the time interval S, was annotated as a RAAP if it represented high RR with itself in the recurrence plot- $RR(S,S) > RR_{thr}$. We set RR_{thr} to 0.75 in this study (see Supplementary Fig. 1 for threshold selection analysis).

2) RAAP Detection in Overlapping Recordings With Cross-Recurrence Plots: Cross-recurrence plots (CRPs) are bivariate recurrence plots. CRPs can visualize repetitive behavior between two systems in the same phase space or a single system at different time intervals [19]. If two catheter positions spatially overlap as in Fig. 1, the electrodes in the overlapping region record similar signals (and activation phase signals) whenever the same RAAP occurs. A CRP calculated on the electrodes of the overlapping area can capture this shared activity.

In our work, we assumed two catheter positions to overlap if at least one of the electrodes of one position was closer to the centroid of the other catheter position than its own. Suppose two overlapping catheter positions p and q from the set of all catheter positions P constitute a set of overlapping electrodes pairs $O^{(p,q)}$:

$$O^{(p,q)} = \{(k,r)\,|\,k \in X_p, r \in X_q, d(k,r) < d_{\max}\}, \quad (5)$$

where X_p is the set of electrode positions of catheter position p, $d(.)$ the distance function between two points on the atria, and $d_{\max}$ the maximum distance between two electrodes. In other words, in the overlapping area, electrodes belonging to different catheter positions (e.g., p and q) were paired with the electrode in the other position that was closer than $d_{\max}$, which was set to 3 mm. In cases where multiple electrodes satisfied this condition, the closest pair was chosen. The activation phase signal distance between catheter positions p and q at time points i and j is then defined as:

$$\delta_{i,j}^{(p,q)} = \frac{1}{2\pi}\cos^{-1}\left(\frac{1}{|O^{(p,q)}|}\sum_{(k,r)\in O^{(p,q)}}\cos\left(\psi_i^k - \psi_j^r\right)\right) \quad (6)$$

The resulting distance matrix among all time points was thresholded to obtain a cross-recurrence plot between two catheter positions p and q:

$$CRP_{i,j}^{(p,q)} = \begin{cases} 0, & \delta_{i,j}^{(p,q)} > \delta_{thr}, \\ 1, & \delta_{i,j}^{(p,q)} \leq \delta_{thr} \end{cases} \quad i = 1,\ldots,T_p; j = 1,\ldots,T_q, \quad (7)$$

where T_p is the number of time points recorded at catheter position p.

3) RAAP Stitching Using an RAAP Connectivity Graph: Detection of RAAPs resulted in a set of RAAP intervals for each catheter position $V = \{I_1, I_2, \ldots, I_P\}$, where I_p represents the RAAP intervals at catheter position p. CRPs were calculated using the methodology introduced in the previous section for every pair of catheter positions with overlapping electrodes. Connected RAAP intervals from multiple catheter positions were represented as an undirected graph, denoted the RAAP connectivity graph, with nodes V (intervals containing RAAPs) and edges E (connected RAAP intervals). The edges were defined as follows:

$$E^{(p,q)} = \left\{\{s,t\}\,|s \in I_p, t \in I_q, RR^{(p,q)}(s,t) \geq RR_{thr}\right\} \quad (8)$$

where $RR^{(p,q)}(s,t)$ represents the recurrence rate operator (given in (4)) applied to the CRP between two catheter locations p and q (see (7)) where repetitive time intervals s and t were observed. The resulting RAAP connectivity graph summarized the network of connected RAAPs that showed a high recurrence rate in respective CRPs. An example is given in Fig. 2(b), where a catheter recorded three positions (depicted by different colors) for 2 s sequentially. RAAPs, shown as square structures on the recurrence plots, were connected if there was a high recurrence rate in the CRP between catheter positions. The resulting RAAP connectivity graph had three nodes, each representing one RAAP from a distinct catheter position. In reality, RAAP connectivity graphs could have many nodes and complex graph topologies, such as multiple connected clusters of nodes. In such cases, we chose the connected component whose nodes spanned to the largest atrial area.

Once the RAAP connectivity graph was obtained, a time point selected at one of the catheter positions could be traced through all the other sites using recurrence plots. For example, a random

time point t_i during RAAP in the purple region showed a connection to time points t_j and t_k in the green and yellow regions, respectively (Fig. 2(b)). This meant that all these time points, although recorded asynchronously, would be snapshots of the same larger RAAP. The activation phase snapshots associated with these time points were stitched to form a composite map as shown in Fig. 2(c).

B. In-Silico Experimental Setting

To replicate clinical data from sequential mapping, we employed a detailed electrophysiological computer model of the atria [22]. This model incorporates a volumetric geometry derived from MRI imaging, augmented with intra- and inter-atrial structures and layer-specific fiber orientations. It enables realistic three-dimensional electrical conduction and can reproduce structural and electrical remodeling, including action potential shortening and fibrosis.

In this work, all simulations had shortened action potentials corresponding to the electrical remodeling that occurs during atrial arrhythmias [22]. Transmembrane potentials were simulated with a spatial resolution of 0.2 mm, from which simulated electrograms were generated by calculating the forward solution. These electrograms were sampled at the sequential positions of the electrodes in a virtual mapping catheter (4 × 4 grid, 3 mm interelectrode distance).

Two sets of simulations were generated to evaluate the composite map algorithm. The first set aimed to reproduce observed conduction patterns in atrial tachyarrhythmias in order to benchmark the ability of the algorithm to reconstruct them. The second set focused on conduction patterns with decreased spatiotemporal stability to evaluate the algorithm's ability to deal with these challenging scenarios.

1) Simulations of Common Stable Activation Patterns: In this set of simulations, five conduction patterns were simulated: a peripheral (single linear) wave, an ectopic focus, multifocal activity, and stable and meandering reentries. Peripheral waves were considered the simplest types of repetitive patterns in terms of spatial complexity and, therefore, utilized as a baseline pattern. A peripheral wave was simulated by pacing the anterior wall of the LA. Ectopic foci were simulated by pacing the left and/or right PV area at a fixed cycle length of 100 ms. Reentries were induced by pacing next to a temporary block line, which was removed after 200 ms. The stable reentry was generated by including a region with scar tissue (diameter: 12 mm) interspersed with conductive paths, which anchored the reentry.

To create the composite maps, the posterior wall between the PVs was sequentially mapped. Electrode grids were manually positioned to achieve approximately 50% overlap between consecutive positions. A total of 30 positions were mapped, and each catheter position was recorded for up to 2 s, resembling typical clinical mapping systems. Temporal misalignment among different catheter positions was introduced by sampling the signals from random starting times at each position.

2) Simulations of Activation Patterns With Variable Spatiotemporal Stability: Conduction patterns with lower spatiotemporal stability pose a challenge to composite mapping. To test the robustness of the proposed algorithm to this dynamic behavior, we generated a set of tachycardia simulations primarily driven by functional reentries and reconstructed the reentry regions with composite maps.

Simulations were conducted in an atrium without and with severe substrate remodeling due to patches of endomysial fibrosis covering 70% of the atria [22]. Incremental pacing (280 to 124 ms) was applied from 20 selected locations in each remodeling group to induce the arrhythmias, which were simulated for 30 s when initiated. The positions of the reentry cores in these simulations were tracked over time based on phase analysis of the transmembrane potentials [23]. The meandering radius of each reentry was quantified as the standard deviation of the unique phase singularity positions around their centroid during the reentry lifespan. Examples of simulations for each group are given in Supplementary Videos 1 and 2.

The regions around the median positions of the reentries lasting longer than 2 s were mapped within a 20 mm radius. To evaluate the impact of overlap, the regions were mapped by positioning the center of the electrode grids at 20, 30, 40, and 50 evenly distributed positions, increasing mapping density. This strategy was chosen to focus the analyses on the most complex patterns present in these simulations. In a clinical mapping procedure, reentry positions are unknown to the operators, but a similar sequential mapping strategy could be employed to localize repetitive patterns. Here, we aimed to assess the optimal mapping density that enables the detection of such conduction patterns.

Electrograms were recorded at each catheter position for 2 s. Due to this recording length and the proposed mapping coverage, it was not feasible to map simulated reentries without allowing for temporal overlap. To mitigate this limitation and still mimic true sequential mapping, we implemented temporal misalignment between recordings by starting recordings from randomly selected time points. This led to misalignment in the phase of the electrograms and changes in the position of the meandering reentry core, thus simulating the expected behavior of mapping a repetitive source. To assess the impact of this data augmentation on the estimated performance, we quantified (i) the correlation between the lifespan of reentries and error metrics and, (ii) the reconstruction performance on a subset of long-lasting reentries (>6 s, mapped 20 locations, 300 ms at each position) that were mapped without any temporal overlap.

C. Evaluation of Composite Maps

Each generated composite map was compared with the actual simulated activation pattern in terms of:

- *LAT error (ms):* Activation phase signal values were converted to LAT values for each composite map using cycle length information. To generate the average LAT map of the ground truth, LAT maps were obtained for each reentry cycle (rotation) and then averaged. Electrodes with missing LAT values were assigned by averaging LAT

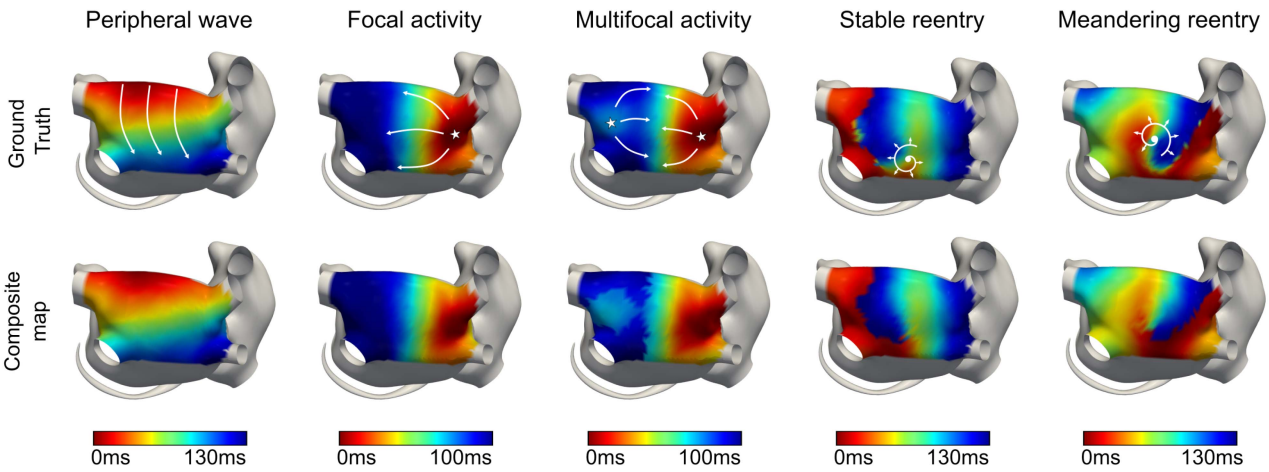

Recurrence rate				
0.98 [0.95-1.00]	0.81 [0.71-0.94]	0.73 [0.65-0.81]	0.70 [0.62-0.81]	0.60 [0.42-0.77]
LAT error (ms)				
3.2 [1.6-4.9] ms	6.5 [3.0-9.6] ms	7.3 [5.3-9.4] ms	8.1 [3.1-12.7] ms	10.3 [3.5-16.2] ms
Conduction direction error (deg):				
5.2 [2.3-8.0] deg.	8.3 [2.1-16.8] deg.	8.5 [1.1-15.9] deg.	9.1 [1.5-19.4] deg.	18.2 [6.7-29.7] deg.

Fig. 3. Composite and actual LAT maps for common stable activation patterns- a single peripheral wave, focal and multifocal firing, a stable reentry and also a meandering reentry. The median and IQR of the LAT and conduction direction errors between each composite map and the actual pattern are given for each mechanism. Recurrence rates for each pattern are also included (median [IQR]) to represent the extent of spatiotemporal organization for each pattern.

values of neighboring electrodes within a 5 mm radius. The median absolute difference between the composite map and the ground truth was calculated. The range of the LAT errors lay between zero and the cycle of a full rotation, which was 130 ms in our study.

- *Conduction direction difference (degrees):* Conduction velocity vectors were computed using the LAT data by a triangulation technique [24]. Only temporally stable conduction direction vectors were retained for the ground truth pattern to avoid highly variable vectors due to the meander of reentries. The stability of a vector was defined as a circular variance of less than 0.5 over all cycles as in [15]. The conduction direction differences were ranging from 0 to 180 degrees.
- *Source localization error (mm):* Conduction vectors were expected to be directed away from the reentry core. Therefore, we localized the position of such sources by vector divergence similar to [25]. Conduction vectors around each anatomical point in a 10 mm radius were projected onto a two-dimensional plane. The divergence of all the projected vectors was computed and assigned to the analyzed anatomical point to represent the likelihood of having a reentry core at this location. The location with the maximum divergence value was labeled as the reentry core. Source localization errors were calculated as the distance between the reentry cores of the actual pattern and the composite map and were, therefore, non-negative values.

Since we only simulated one instance for each common stable activation pattern, error distributions for common stable conduction patterns were obtained by aggregating the errors obtained at each electrode location together. Additionally, calculations of core localization error for these stable patterns were omitted, as this metric did not apply to peripheral waves. LAT and conduction errors for common conduction patterns were analyzed using the Kruskal-Wallis nonparametric test with Tukey's honestly significant difference procedure for multiple comparisons.

For simulated meandering reentries, we obtained error distributions by aggregating average errors from each simulated reentry. To investigate how error metrics relate to the spatiotemporal instability of the underlying patterns, we employed straightforward linear regression models to analyze the connection between meandering areas and errors. The coefficients of these models were standardized, ensuring that the slope directly represents the correlation coefficient. Our results were presented using median values and the lower and upper quartile.

III. Results

A. Stable Patterns Were Reconstructed With Minimal Errors

Multiple repetitive mechanisms were reconstructed with the proposed algorithm. The resulting composite maps closely resembled the actual activation patterns in each instance and effectively represented the mapped mechanisms (Fig. 3). A repetitive single peripheral wave, the simplest simulated pattern, could be

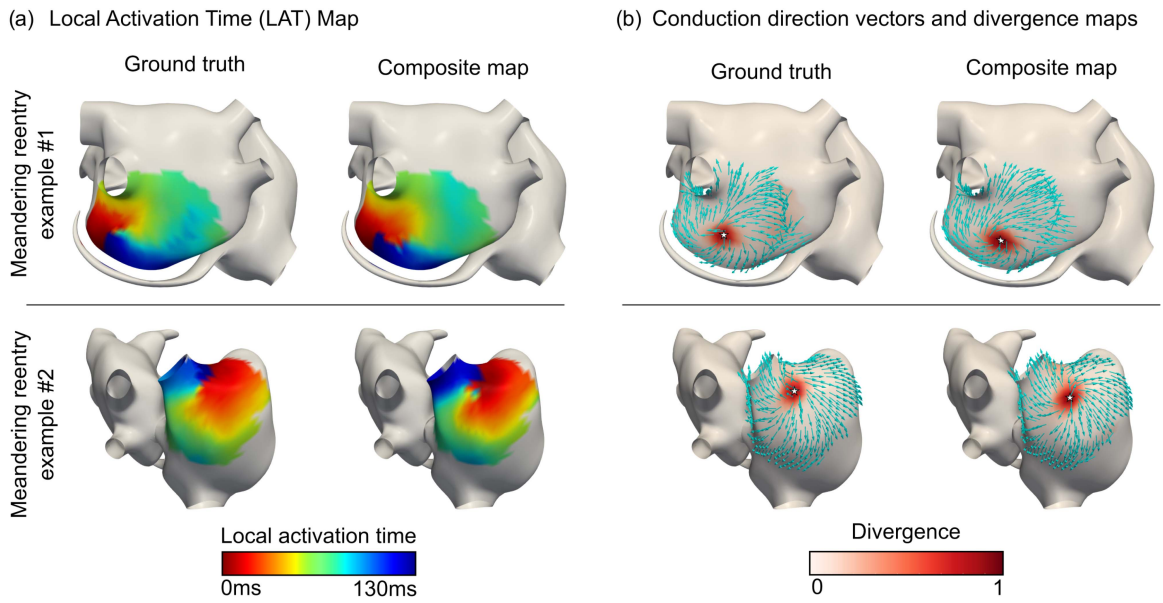

Fig. 4. Two composite maps generated for meandering reentries when 30 locations around the reentry core were mapped. (a) Local activation time (LAT) maps of and (b) conduction direction vector and associated divergence maps. Stars represent the maximum divergence points.

reconstructed with the smallest LAT and conduction direction errors (3.2 [1.6–4.9] ms and 5.2 [2.3–8.0] deg., respectively). Comparatively, other localized patterns, such as focal, multifocal firing, and stable reentry, presented slightly higher errors (LAT errors: 6.5 [3.0–9.6] ms, 7.3 [5.3–9.4] ms, 8.1 [3.1–12.7] ms and conduction direction errors: 8.3 [2.1–16.8] deg., 8.5 [1.1–15.9] deg., 9.1 [1.5–19.4] deg., respectively.). The differences in error values between these patterns and the peripheral waves were significant, but not amongst themselves ($p<0.05$, nonparametric Kruskal-Wallis test with Tukey's HSD test). Errors were the highest for the unstable meandering reentry (10.3 [3.5–16.2] ms and 18.2 [6.7–29.7] deg.); $p<0.05$).

B. Reconstruction of Unstable Reentries

111 unstable reentries, each lasting longer than 2 s, were mapped sequentially. The lifespan of these reentries was 3.0 [2.4–4.8] s. These reentries meandered in an area with a radius of 3.3 ± 1.3 mm, with a cycle length of 138 ± 7 ms. Mapping 20, 30, 40, and 50 locations around each reentry core resulted in an average overlap of 3.2 ± 0.6 ($20\pm4\%$ of the mapping catheter), 4.5 ± 0.6 ($28\pm4\%$), 5.3 ± 0.5 ($33\pm3\%$), and 6.1 ± 0.5 ($38\pm3\%$) electrodes, respectively. Some examples of the reconstructed composite maps with the associated actual activation maps are given in Fig. 4 for sequentially mapping 30 positions around the reentry core. In each example, LAT, conduction direction information, and maximum divergence point of the generated composite map resembled those of the actual pattern.

For unstable patterns, LAT and conduction direction errors were significantly higher for the cases where 20 locations around the phase singularity were mapped than those with 30, 40, and 50 locations (For LAT error: $p < 0.03$, $p < 0.02$, and $p < 0.0001$ respectively; for conduction direction errors: $p < 0.0001$, $p < 0.0001$, and $p < 0.00001$, Kruskal-Wallis test with Tukey's HSD test). No significant difference in LAT and conduction direction errors were observed among 30, 40, and 50 locations (Fig. 5(b), left and middle).

We did not observe any correlation between the lifespan of reentries and the error metrics (Supplementary Fig. 2). Moreover, true sequential mapping of a small subset of long-lasting reentries showed no increased errors compared to our data augmentation approach (Supplementary Fig. 3).

There were no significant differences in core localization errors between the cases where 20, 30, 40, and 50 locations were mapped (Fig. 5(b), right). Based on the observation that no significant improvement in the errors was observed by further increasing recording density to more than 30 locations, 30 locations around each phase singularity were chosen as the optimal mapping configuration for composite mapping. LAT errors for this configuration were -6.1 [4.2–8.6] ms. LAT errors were upper-bounded by 15.2 ms (Fig. 6, top). Conduction direction errors were, on average- 11.2 [8.6–15.5] degrees and upper-bounded by approximately 31 degrees (Fig. 6, middle). Lastly, source localization errors were, on average, 4.1 [2.9–4.9] mm with an upper boundary of 8 mm (Fig. 6, bottom). LAT, conduction direction, and reentry core localization errors were weakly correlated with the meandering area ($\rho = 0.41$ ($p = 8e\text{-}06$); $\rho = 0.40$ ($p = 2e\text{-}05$) and $\rho = 0.20$ ($p = 4e\text{-}02$), respectively).

IV. Discussion

In this study, we demonstrated that our composite mapping technique can be used reliably to reconstruct clinically relevant conduction patterns in a realistic in-silico setting. The proposed algorithm eliminated the necessity for a coronary sinus reference catheter by focusing solely on the overlapping activity between catheter positions. We also reached an optimal mapping strategy

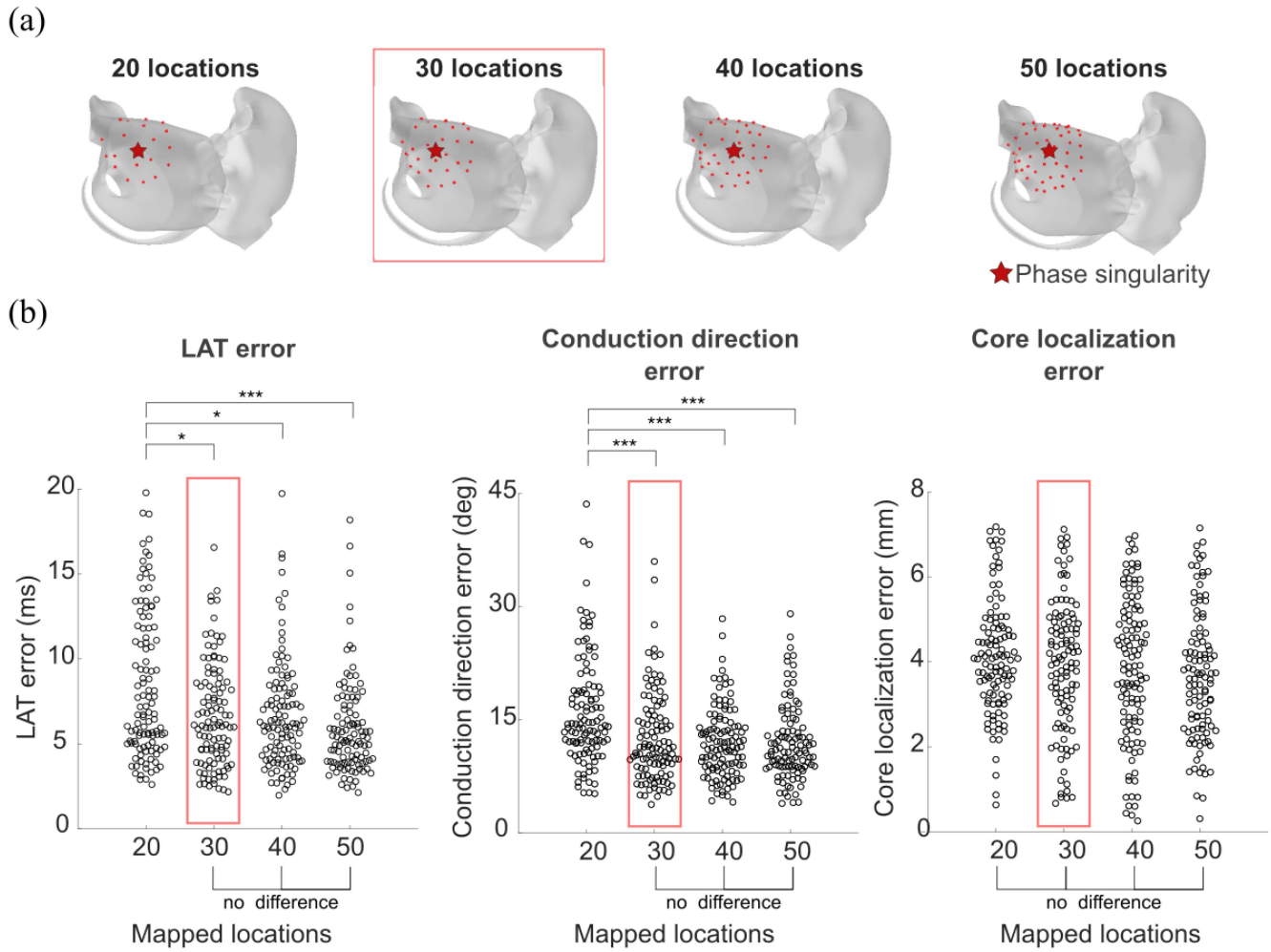

Fig. 5. Composite map errors in local activation time (LAT), conduction direction, and reentry core localization. (a) The mapping strategy for unstable reentries: The surroundings of each detected phase singularity that lasted more than 2 seconds were mapped. Catheter centroids (red dots) were homogenously chosen around each phase singularity- 20, 30, 40, and 50 catheter positions were mapped. (b) Error distributions were given for each different mapping density. Cases were statistically compared (*: $p < 0.05$, ***: $p < 0.001$). The red frame displays the results obtained for the N = 30 case used in the following analyses of this study.

regarding the minimum required number of positions around a meandering reentry.

A. Composite Mapping as a Tool to Visualize Atrial Arrhythmia Mechanisms

The rise in the number of ablation procedures, which have been demonstrated as a safe first-line treatment for rhythm control in AF and AFL patients [1], also leads to an increased number of atypical post-ablation reentrant circuits [26]. Consequently, electroanatomical mapping is becoming an increasingly relevant tool for the treatment of such atrial arrhythmias, aiming to localize conduction patterns that can act as sources for the arrhythmic conduction and may be complementary ablation targets [26], [27]. However, localizing these drivers poses a great challenge for electrophysiologists since the current technology faces limitations in spatial coverage or resolution while mapping these dynamic conduction patterns [6]. The composite mapping algorithm proposed here was conceived to address this technical challenge for patients whose atrial tachyarrhythmias are maintained by repetitive localized sources, even if intermittently.

In this respect, this work explores repetitive activity as a marker of underlying mechanisms characterized by a certain degree of organization. We hypothesize that source-like mechanisms that hierarchically drive atrial tachyarrhythmias are responsible for the RAAPs in the surrounding area, which may convert into fibrillatory conduction in the distant locations [17], [27]. Focusing on RAAPs could help filter out this more disorganized activity, improving the likelihood of finding potential localized mechanisms. Such repetitive patterns are the primary driving mechanism during AFL and focal tachycardia, and repetitive patterns have been observed in AF in both animal [28] and human studies [15], [20]. However, their presence and stability are still disputed and may vary between AF patients [29].

The composite mapping technique is envisioned as an additional functionality of the existing mapping software, provided multiple positions across atria are mapped densely with overlap. Prior knowledge of a driver's location is not required for

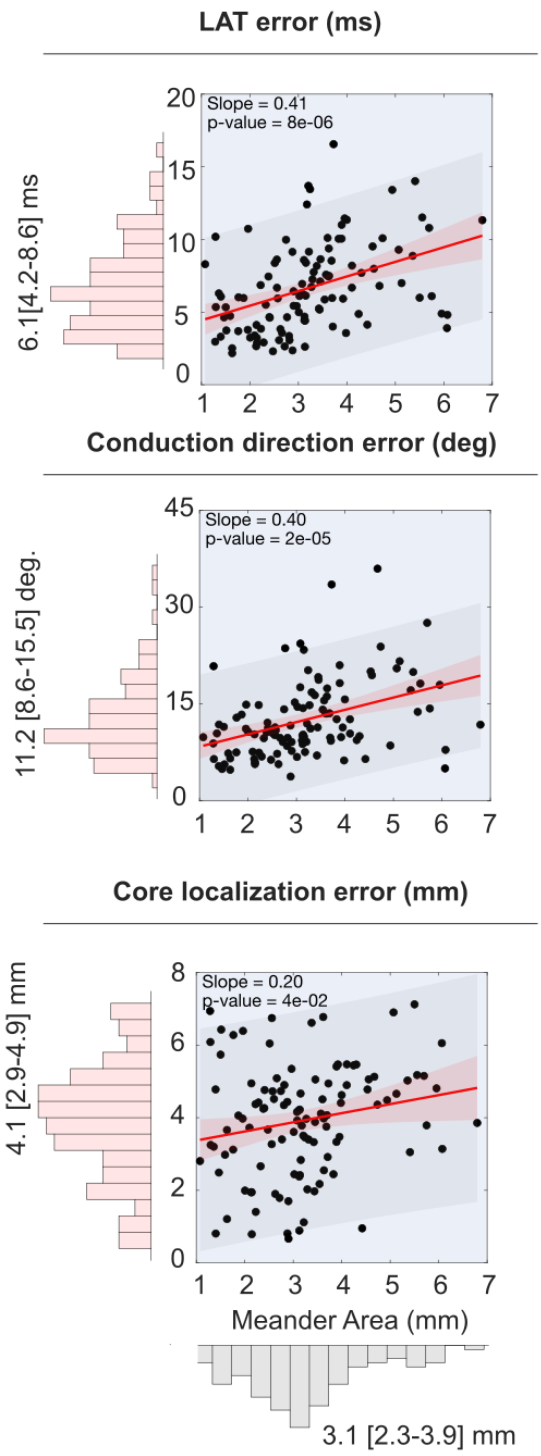

Fig. 6. Detailed results for 30 locations: Histograms of errors and scatter plots of meander area versus errors for each phase singularity. Shaded areas represent prediction intervals (95%). The slope of the fitted linear line and the associated p-value were given in each scatter plot.

composite mapping. The proposed algorithm can detect local repetitive activity and stitch it together with activities at adjacent catheter locations if they share a similar propagation pattern in the overlapping area.

An RAAP must appear at least once during the mapping of each catheter position to be included in the composite map. Our algorithm is tailored to identify patterns that are either constantly present or appear intermittently yet regularly. Generating a composite map for short-lived transient repetitive patterns is outside the scope of our approach, because ablation of the area characterized by such a pattern may not be beneficial to terminate arrhythmia. Extending the mapping duration could improve the likelihood of capturing the same RAAP across various locations. While this approach leads to increased procedure times, previous research showed the feasibility of mapping the atria at 35 locations for 30 seconds at each site [30].

The presented algorithm effectively reconstructed composite maps for multiple common conduction patterns, achieving minimal LAT and conduction direction errors and high visual resemblance to the actual patterns. We used the simplest pattern simulated, a single peripheral wavefront, as a baseline in our statistical analyses. This decision was based on the fact that a large wavefront propagating in a single direction would be more repetitive and less affected by LAT annotation ambiguities, frequently observed in areas with more complex conduction, such as the reentry cores and points of wave collision and pivoting. This expectation was verified by the high recurrence rate of the peripheral pattern compared to the other patterns (see Fig. 3). Despite the simplicity of the pattern, detecting peripheral waves during less organized arrhythmias is not a trivial task and may lead to important therapeutic implications. Our group recently demonstrated the association between the percentage of peripheral waves and the overall complexity of arrhythmia [15]. Moreover, a positive outcome of PVI was associated with peripheral waves originating from the pulmonary veins in AF patients [31]. Composite maps may be instrumental in observing peripheral wave distribution and potentially stratifying patients, leading to more personalized treatments.

The current protocols for mapping stable arrhythmias (AFL and focal tachycardia) include sequential mapping with a CS catheter serving as a reference [32]. Our proposed strategy offers an alternative that only relies on one catheter to generate composite maps, without requiring additional reference catheters. This feature is particularly advantageous with the decrease in arrhythmic organization, which may lead to an uncoupling between the reference catheter and the mapped region, yielding unreliable reconstructions. Our approach, on the other hand, uses the signals from the overlapping mapping areas as local references. This method is expected to mitigate the uncoupling between the reference and the mapping catheters while preventing the disadvantages of using additional reference catheters, such as the additional cost, the need for additional transseptal punctures, and catheter stabilization issues. The added value of not using a reference catheter could be quantified by a benchmark study with RADAR approach [11], which utilizes a CS reference catheter for electrogram alignment. However, the algorithmic details of the RADAR approach stay undisclosed.

B. Effect of Pattern Instability on Composite Maps Performance

The increase in spatiotemporal instability, represented here by the meandering reentries, only mildly affected the composite map reconstruction quality. The effect was associated with reduced repetitive activity around the reentry core. Since a meandering reentry completes each rotation at a different location, none of the consecutive cycles presents repetitive activity around the core. Consequently, LAT information for these meandering areas comes from interpolating the LATs in the vicinity, which deviates from the actual values. This procedure leads to increased errors in this area, which are more pronounced with larger meandering areas. Despite this limitation, source localization errors were upper-bounded when a sufficient mapping density was obtained. While the accuracy required for targeting reentries during ablation is unknown, our results suggest that composite mapping may be accurate enough for the available clinical tools. Current ablation catheters deliver lesions of approximately 5 to 7 mm [33]. In our analyses, 98% of the true reentry cores were within this upper limit, indicating that sources localized by composite mapping would be frequently ablated accurately.

Reentries may meander in areas larger than observed in the simulation or may not be contained to a particular area [18]. The dynamics of a rotor, such as its trajectory, speed, and wavelength, are closely related to the electrical and substrate heterogeneity of the myocardium [34]. In such cases where the trajectory of a reentry is random or not repetitive, a composite map cannot be reconstructed.

C. Effect of Spatial Overlap on Performance

The greater the overlap between two catheter positions, the more evidence can be obtained to align and stitch RAAPs detected at these positions. A larger number of electrograms from the overlapping region leads to more reliable cross-recurrence plot estimates and enables better signal alignment over different catheter positions. In our simulated dataset of unstable reentries, the minimally chosen overlap of 20 locations led to the worst result ($20 \pm 4\%$ spatial overlap; 3.2 ± 0.6 electrodes). The result improved for 30 locations corresponding to $28 \pm 4\%$ spatial overlap (4.5 ± 0.6 electrodes), with no further improvement observed beyond this value. Consequently, this minimum overlap of 5 electrodes might be required to provide sufficient information for merging RAAPs into a composite map. However, more overlap could be warranted in more complex recordings with many different RAAPs.

It should be noted that the employed catheter was a regularly spaced grid; therefore, a particular overlapped area corresponds to a fixed number of electrodes. This will not be the case for non-uniform grids, for which the minimum overlap requirement should be reassessed.

D. Data Augmentation and the Effect of Temporal Overlap

Our data augmentation approach introduces temporal overlap between recordings, but the selection of random time intervals prevents exact temporal alignment. This temporal overlap could underestimate the errors made by the composite mapping algorithm in a clinical setting. However, our results suggested otherwise. First, we tested the relationship between the amount of temporal overlap and the reconstruction error by correlating the error to the lifespan of reentries. The lack of correlation indicated that our data augmentation approach was not oversimplifying the process. Our second experiment, where we emulated sequential mapping for a small number of reentries with longer durations ($>$6 s), also showed no difference between the results obtained by data augmentation and actual sequential mapping. These two experiments, taken together, showed that the data augmentation scheme used in this study did not underestimate errors despite its simplification of the problem.

V. Limitations

While the simulations used in this study reflect many of the conduction patterns observed during atrial tachyarrhythmias, including transient functional reentries, endo-epicardial dissociation, and transmural breakthroughs, our computer model cannot fully represent the arrhythmia complexity of all patients. Due to limitations in computational resources, the duration of the simulations was not long enough to enable true sequential mapping without data augmentation or to frequently observe reentries that disappear and reappear at the same locations. Consequently, the proposed methods require validation in clinical settings to assess their performance accurately.

A major limitation of composite mapping is the prolonged procedural duration due to mapping the entire atria with overlaps. Our previous research [15] demonstrated that certain patients might display highly complex electrograms with a small number of RAAPs. For these patients, procedural duration might even be longer to capture RAAPs. Furthermore, challenges in endocardial mapping, such as poor electrode contact, might adversely affect the quality of the composite maps. In atrial locations with inadequate electrode contact, identifying LATs may become infeasible, leading to impaired RAAP detection [35]. As a result, these areas may not contribute to the composite map, diminishing its spatial coverage and potentially lessening the mechanistic insights it can offer. To assess the impact of this issue, a subsequent in-silico study designed to replicate scenarios of poor electrode contact would be beneficial.

Our analysis was limited to a specific catheter design, while various high-density options like the PentaRay (Biosense Webster, Inc.) are used in practice, which, with its star-like, flexible splines and 20 uneven electrodes, adds complexity to electrode comparisons. Hence, additional studies are needed to assess the impact of different catheter designs on the accuracy of composite mapping.

VI. Conclusion

The proposed composite mapping algorithm could accurately reconstruct simulated stable and unstable patterns that resembled the driver mechanisms of atrial tachyarrhythmias. Errors were higher for meandering reentries, although the detected reentry cores were consistently close to the actual locations. Composite maps offer a unique opportunity to summarize, with both high-density and high-coverage, the conduction activity associated with the most repetitive patterns in patients with atrial arrhythmias where they are present. Such imaging could have a significant impact on mechanistic ablation studies for patients who experience recurrences after initial ablations. A natural progression of this work is to conduct an ablation trial based on the localized drivers identified by the composite maps.

References

[1] J. A. Joglar et al., "2023 ACC/AHA/ACCP/HRS guideline for the diagnosis and management of atrial fibrillation: A report of the american college of cardiology/american heart association joint committee on clinical practice guidelines," *Circulation*, vol. 149, no. 1, pp. e1–e156, 2024.

[2] R. Parameswaran, A. M. Al-Kaisey, and J. M. Kalman, "Catheter ablation for atrial fibrillation: Current indications and evolving technologies," *Nature Rev. Cardiol.*, vol. 18, no. 3, pp. 210–225, 2021.

[3] T. Rostock et al., "Characterization, mapping, and catheter ablation of recurrent atrial tachycardias after stepwise ablation of long-lasting persistent atrial fibrillation," *Circulation: Arrhythmia Electrophysiol.*, vol. 3, no. 2, pp. 160–169, 2010.

[4] S. Yamashita et al., "Atrial tachycardias: Cause or effect with ablation of persistent atrial fibrillation?," *J. Cardiovasc. Electrophysiol.*, vol. 29, no. 2, pp. 274–283, 2018.

[5] P. Compagnucci et al., "Recent advances in three-dimensional electroanatomical mapping guidance for the ablation of complex atrial and ventricular arrhythmias," *J. Interventional Cardiac Electrophysiol.*, vol. 61, pp. 37–43, 2021.

[6] C. H. Roney et al., "Spatial resolution requirements for accurate identification of drivers of atrial fibrillation," *Circulation: Arrhythmia Electrophysiol.*, vol. 10, no. 5, 2017, Art. no. e004899.

[7] P. A. Friedman, "Novel mapping techniques for cardiac electrophysiology," *Heart*, vol. 87, no. 6, pp. 575–582, 2002.

[8] B. King et al., "Effect of spatial resolution and filtering on mapping cardiac fibrillation," *Heart Rhythm*, vol. 14, no. 4, pp. 608–615, 2017.

[9] M. T. Pope et al., "Spatial and temporal variability of rotational, focal, and irregular activity: Practical implications for mapping of atrial fibrillation," *J. Cardiovasc. Electrophysiol.*, vol. 32, no. 9, pp. 2393–2403, 2021.

[10] Y. Wang et al., "Noninvasive electroanatomic mapping of human ventricular arrhythmias with electrocardiographic imaging," *Sci. Transl. Med.*, vol. 3, no. 98, pp. 98ra84–98ra84, 2011.

[11] S. Choudry et al., "RADAR: A multicenter food and drug administration investigational device exemption clinical trial of persistent atrial fibrillation," *Circulation: Arrhythmia Electrophysiol.*, vol. 13, no. 1, 2020, Art. no. e007825.

[12] N. Vandersickel et al., "Directed networks as a novel way to describe and analyze cardiac excitation: Directed graph mapping," *Front. Physiol.*, vol. 10, p. 1138, 2019, doi: 10.3389/fphys.2019.01138.

[13] J. Duchateau et al., "Performance and limitations of noninvasive cardiac activation mapping," *Heart Rhythm*, vol. 16, no. 3, pp. 435–442, 2019.

[14] O. Özgül et al., "High-density and high coverage composite mapping of repetitive atrial activation patterns," *Comput. Biol. Med.*, vol. 159, 2023, Art. no. 106920.

[15] F. van Rosmalen et al., "Incidence, prevalence, and trajectories of repetitive conduction patterns in human atrial fibrillation," *EP Europace*, vol. 23, no. Supplement_1, pp. i123–i132, 2021.

[16] S. Zeemering et al., "A novel tool for the identification and characterization of repetitive patterns in high-density contact mapping of atrial fibrillation," *Front. Physiol.*, vol. 11, 2020, Art. no. 570118.

[17] S. M. Narayan, D. E. Krummen, and W.-J. Rappel, "Clinical mapping approach to diagnose electrical rotors and focal impulse sources for human atrial fibrillation," *J. Cardiovasc. Electrophysiol.*, vol. 23, no. 5, pp. 447–454, 2012.

[18] S. Nattel, F. Xiong, and M. Aguilar, "Demystifying rotors and their place in clinical translation of atrial fibrillation mechanisms," *Nature Rev. Cardiol.*, vol. 14, no. 9, pp. 509–520, 2017.

[19] N. Marwan et al., "Recurrence plots for the analysis of complex systems," *Phys. Rep.*, vol. 438, no. 5/6, pp. 237–329, 2007.

[20] B. J. Hermans et al., "Selecting repetitive focal and rotational activation patterns with the highest probability of being a source of atrial fibrillation," *J. Mol. Cellular Cardiol. Plus*, vol. 7, 2024, Art. no. 100064.

[21] S. Zeemering et al., "Automated quantification of atrial fibrillation complexity by probabilistic electrogram analysis and fibrillation wave reconstruction," in *Proc. IEEE Annu. Int. Conf. Eng. Med. Biol. Soc.*, 2012, pp. 6357–6360.

[22] A. Gharaviri et al., "Epicardial fibrosis explains increased endo–Epicardial dissociation and epicardial breakthroughs in human atrial fibrillation," *Front. Physiol.*, vol. 11, p. 68, 2020, doi: 10.3389/fphys.2020.00068.

[23] R. Zou et al., "Development of a computer algorithm for the detection of phase singularities and initial application to analyze simulations of atrial fibrillation," *Chaos: An Interdiscipl. J. Nonlinear Sci.*, vol. 12, no. 3, pp. 764–778, 2002.

[24] B. Verma et al., "Regional conduction velocity calculation from clinical multichannel electrograms in human atria," *Comput. Biol. Med.*, vol. 92, pp. 188–196, 2018.

[25] M. Masè et al., "A divergence-based approach for the identification of atrial fibrillation focal drivers from multipolar mapping: A computational study," *Front. Physiol.*, vol. 12, 2021, Art. no. 749430.

[26] A. Chugh, "Mapping and ablation of post-AF atrial tachycardias," *J. Cardiovasc. Electrophysiol.*, vol. 32, no. 10, pp. 2830–2844, 2021.

[27] J. G. Quintanilla et al., "Novel approaches to mechanism-based atrial fibrillation ablation," *Cardiovasc. Res.*, vol. 117, no. 7, pp. 1662–1681, 2021.

[28] A. Van Hunnik et al., "Stationary atrial fibrillation properties in the goat do not entail stable or recurrent conduction patterns," *Front. Physiol.*, vol. 9, p. 947, 2018, doi: 10.3389/fphys.2018.00947.

[29] D. Dharmaprani et al., "Renewal theory as a universal quantitative framework to characterize phase singularity regeneration in mammalian cardiac fibrillation," *Circulation: Arrhythmia Electrophysiol.*, vol. 12, no. 12, 2019, Art. no. e007569.

[30] M. Wolf et al., "Identification of repetitive atrial activation patterns in persistent atrial fibrillation by direct contact high-density electrogram mapping," *J. Cardiovasc. Electrophysiol.*, vol. 30, no. 12, pp. 2704–2712, 2019.

[31] C. H. Roney et al., "Time-averaged wavefront analysis demonstrates preferential pathways of atrial fibrillation, predicting pulmonary vein isolation acute response," *Front. Physiol.*, vol. 12, 2021, Art. no. 707189.

[32] N. Habel et al., "The temporal variability of dominant frequency and complex fractionated atrial electrograms constrains the validity of sequential mapping in human atrial fibrillation," *Heart Rhythm*, vol. 7, no. 5, pp. 586–593, 2010.

[33] S. M. Narayan et al., "Treatment of atrial fibrillation by the ablation of localized sources: Confirm (conventional ablation for atrial fibrillation with or without focal impulse and rotor modulation) trial," *J. Amer. College Cardiol.*, vol. 60, no. 7, pp. 628–636, 2012.

[34] C.-H. Xu et al., "Rotor mechanism and its mapping in atrial fibrillation," *Europace*, vol. 25, no. 3, pp. 783–792, 2023.

[35] J. M. de Bakker, "Electrogram recording and analyzing techniques to optimize selection of target sites for ablation of cardiac arrhythmias," *Pacing Clin. Electrophysiol.*, vol. 42, no. 12, pp. 1503–1516, 2019.